ACS Sustainable Chemistry & Engineering

pubs.acs.org/journal/ascecg

Research Article

Selective Oxidation of Biomass-Derived 5-Hydroxymethylfurfural Catalyzed by an Iron-Grafted Metal−Organic Framework with a Sustainably Sourced Ligand

Satarupa Das, Giannantonio Cibin, and Richard I. Walton*

Cite This: ACS Sustainable Chem. Eng. 2024, 12, 5575−5585

Read Online

ACCESS | Metrics & More | Article Recommendations | Supporting Information

ABSTRACT: The efficient conversion of biomass-derived 5-hydroxymethylfurfural (HMF) to 2,5-furandicarboxylic acid (FDCA) is a major challenge under base-free conditions with inexpensive catalysts. We report a precious-metal-free recyclable MOF-based catalyst (CAU-28), constructed from the FDC ligand, with grafted redox-active Fe sites. This enables the conversion of HMF to FDCA under solvothermal heating or microwave-assisted methods in base-free aqueous conditions. The optimized process achieves 100% HMF conversion producing FDCA at the gram scale with a 70−80% yield in 1 h. The turnover frequency (TOF) and cost-normalized TOF for the best catalyst are >800 h^{-1} and >1000 h^{-1} $£^{-1}$, respectively, surpassing those of conventional catalysts and processes using precious elements or basic additives for HMF conversion. The economic viability and practical applicability of the process are further realized by utilizing the catalytically derived FDCA (without purification) for the successful construction of pristine CAU-28 MOFs and formation of the biodegradable plastic polyethylene furanoate (PEF) after purification.

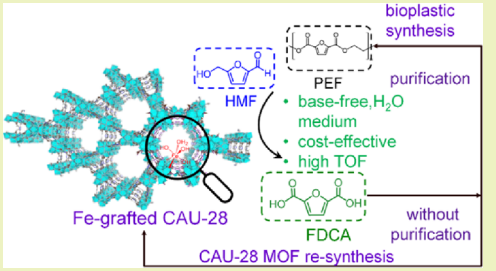

KEYWORDS: *iron grafting, MOF catalyst, biomass conversion, catalytic oxidation, 2,5-furan dicarboxylic acid*

INTRODUCTION

The continued consumption of nonrenewable, fossil-based resources for industrial fuel and chemical production has severe adverse environmental impacts along with cost inefficiency that will become more pressing as the sources are deplenished.[1] The transition to green and sustainable feedstocks is therefore imperative for chemical sectors in the near future.[2,3] Lignocellulosic biomass (comprising cellulose, hemicellulose, and lignin fractions) holds great potential as an alternative feedstock to the rapidly depleting petroleum-based resources owing to its abundance and low cost.[4] Among various biomass derivatives, 5-hydroxymethylfurfural (HMF) is considered as a highly valuable intermediate that can be sourced from cellulose (Figure 1a,b).[4] Although there are challenges in optimizing the production of HMF due to its relative instability at higher temperatures and separation from side products, it has been widely publicized as a high-value platform chemical.[5] Industrial production of HMF has proven viable, and this can be anticipated to lead to a reduction in its cost.[6] The oxidation of HMF yields a range of useful products, with 2,5-furandicarboxylic acid (FDCA) being of particular interest and commercial value.[7] FDCA is potentially lucrative for the chemical industry as it is a substitute for the commonly used benzene-1,4-dicarboxylic acid (terephthalic acid), which is sourced from fossil-based organics, specifically via the oxidation of *para*-xylene,[8] and used primarily for the production of nonbiodegradable polyethylene terephthalate (PET) plastics.[9] The polymerization of biomass-derived FDCA and ethylene glycol results in the formation of polyethylene furanoate (PEF), a biodegradable plastic that exhibits comparable structural and physiochemical properties to those of PET.[10] In fact, PEF plastics have superior barrier properties and higher resistance to heat and gas permeation compared to PET, making them more appealing for commercial adoption.

Obtaining FDCA from biomass-derived HMF involves several challenges.[11] The oxidation of HMF to FDCA proceeds via stepwise reactions involving the oxidation of both alcohol and aldehyde functional groups present in HMF.[12] The design of catalysts for facilitating the process with a high efficacy and selectivity is therefore critical. In recent years, various methods have been reported for the oxidation of HMF, including processes based on homogeneous, heterogeneous, and enzyme-based catalysts.[13−16] However, in most cases, the catalysts suffer from poor stability or contain scarce precious metals, thereby limiting their applicability on an industrial scale.[17−20] The reaction medium for catalytic HMF conversion typically also requires the use of ionic liquids or bases (e.g., NaOH, Na_2CO_3, and K_2CO_3) to improve the overall

Received: December 28, 2023
Revised: February 23, 2024
Accepted: March 14, 2024
Published: March 25, 2024

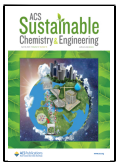

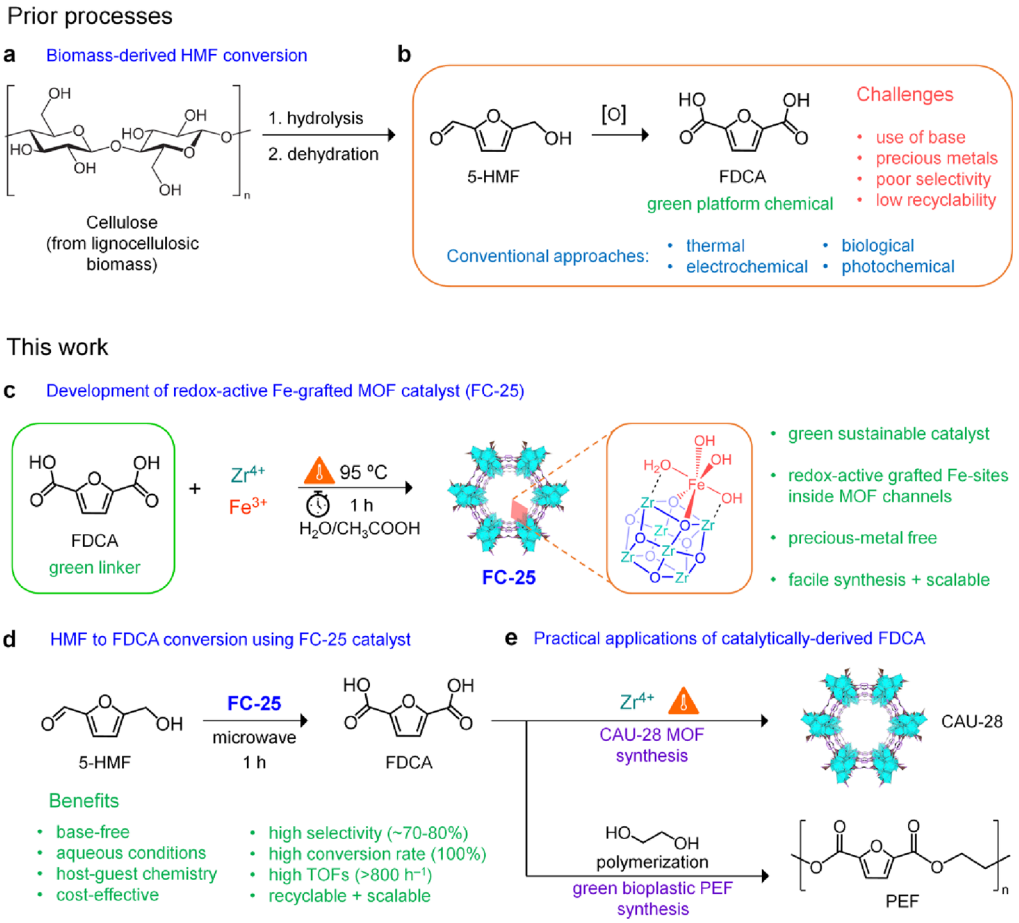

Figure 1. Overview of the existing HMF to FDCA conversion processes and new strategies explored in this work. (a,b) Schematic of biomass-derived HMF conversion indicating the commonly used methods and their existing limitations. (c) Construction of MOF catalysts species with grafted redox-active sites. (d,e) HMF conversion and its benefits using the developed catalyst system (d) and further applications explored using the catalytically derived FDCA (e).

efficiency, but this makes the process unsustainable and expensive.[21−24] The use of these reagents also makes the purification and separation of the FDCA challenging, clearly indicating that an alternative approach is needed. Additionally, most HMF conversion reactions operate under harsh and energy-intensive conditions (high temperatures, long durations, or oxygen pressures), further preventing the process from being economically viable.[25,26] Therefore, the development of precious-metal-free systems, which can efficiently catalyze the scalable production of FDCA under mild, base-free aqueous conditions, is essential to realize the full potential of FDCA as a sustainable building block for chemical synthesis.

In recent times, metal−organic frameworks (MOFs) have gained significant attention owing to their ultrahigh surface areas and tunable porosity.[27,28] The ease of functionalization of MOFs makes use of metals from all parts of the Periodic Table, combined with ligands of diverse functionalities that can be modified, either pre- or postsynthesis, to give bespoke properties for heterogeneous catalysis.[29] However, despite these attractive features, MOF-based catalysts have not been widely explored for aerobic and base-free HMF oxidation reactions possibly due to the challenge in engineering MOFs with suitable stability and robust redox-active sites to efficiently convert HMF to FDCA,[30,31] which are also stable to withstand prolonged exposure to polar reagent molecules and solvents above room temperature. Additionally, most MOFs are constructed from ligands that are either derived from fossil fuels or custom-made using lengthy processes. Hence, using MOF catalysts with the sustainable, biomass-derived 2,5-furandicarboxylate (FDC) linker (i.e., the deprotonated form of FDCA) holds great promise.[32]

In this work, an MOF based on earth-abundant Zr metal and FDC linkers (CAU-28) is grafted with Fe^{3+} redox sites, which act as effective catalytic sites for the base-free and scalable conversion of HMF to FDCA under conventional or microwave-assisted heating with high yields and turnovers (Figure 1c,d). The CAU-28 MOF serves as an ideal choice as the catalytic host matrix owing to its facile aqueous-based synthesis approach, the use of sustainably sourced FDC linkers, and the presence of large pores/channels that can house the redox-active species facilitating catalysis via enhanced substrate−catalyst interactions. Another important reason for selecting this material as a host is that it is well-known that MOFs based on the Zr_6 cluster are among the most stable toward the solvent and temperature. The grafted Fe species and their role in selective HMF oxidation with no need for base additives have been probed using detailed characterization and analytical approaches. Furthermore, the catalytically derived FDCA (from HMF) was successfully applied for the construction of further batches of CAU-28 MOFs and also allowed for the synthesis of the bioplastic PEF (Figure 1e), thereby demonstrating the commercial benefits and practicality

https://doi.org/10.1021/acssuschemeng.3c08564
ACS Sustainable Chem. Eng. 2024, 12, 5575−5585

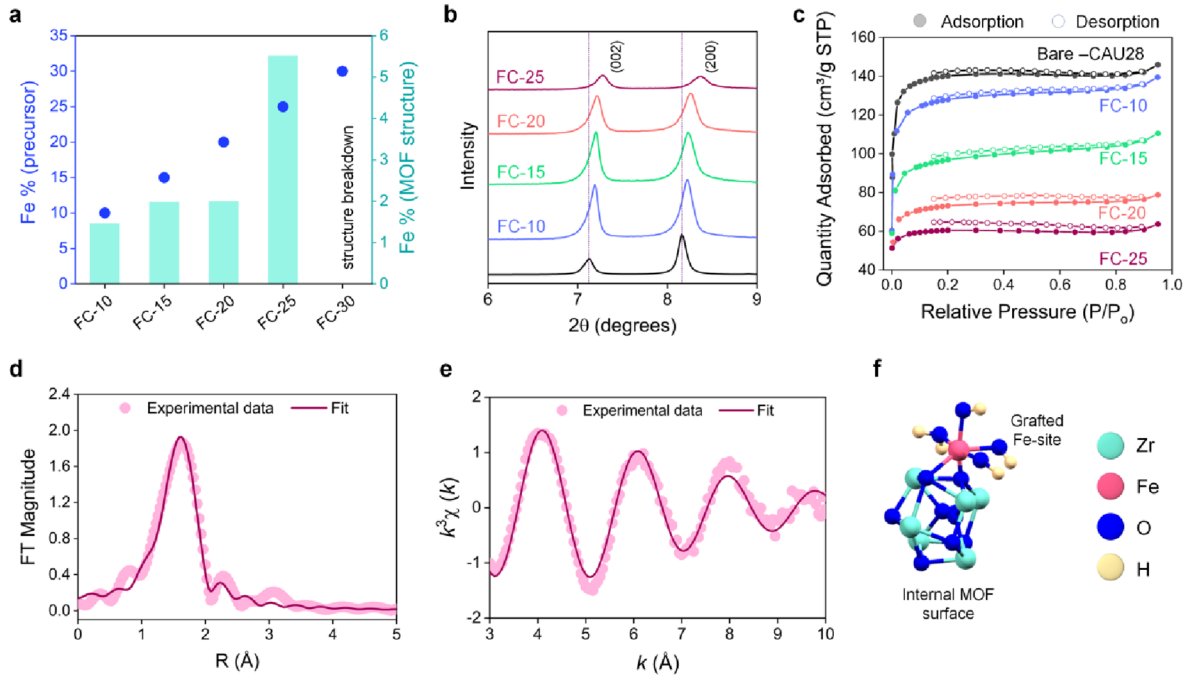

Figure 2. Characterization of the FC catalyst systems. (a) Comparison between the intended and actual Fe loading in the CAU-28 MOF structure as determined using XRF analysis. (b) PXRD patterns of the different FC systems indicating the shift in the major reflections with Fe inclusion. The black pattern indicates the simulated pattern of the parent CAU-28 MOF. (c) N_2 isotherms of the different FC systems for determination of the surface area. (d,e) Fe K-edge EXAFS spectroscopic analyses for the catalyst, FC-25 showing the k^3-weighted EXAFS spectrum, and (e) associated Fourier transform. (f) Structural representation of the Fe grafting on the Zr oxo-cluster present in the MOF.

of the process that might contribute toward a sustainable circular economy.

RESULTS AND DISCUSSION

The hydrothermally stable CAU-28 MOF consists of ($[Zr_6O_4(OH)_4]$) clusters and FDC ligands.[33] The presence of the abundant and nontoxic metal Zr and the sustainably sourced FDC linkers makes CAU-28 an attractive candidate for catalytic applications, although it has not been explored in the literature for this purpose. CAU-28 has a framework that exhibits two types of channels. Larger hexagonal channels have a diameter of ~16 Å, while smaller channels have a diameter of ~3 Å. (Figure S1). It therefore has the potential as a host for housing redox-active catalytic species/sites for efficient catalytic transformations by enabling effective substrate−catalyst interactions. Following this principle, we aimed to incorporate redox-active Fe^{3+} species into the CAU-28 structure for imparting catalytic activity for HMF oxidation (discussed in later sections).

The Fe-incorporated CAU-28 MOFs were synthesized via a modified method using a mild solvothermal process (see Methods for details), which was optimized by varying the reaction duration and temperature. The material with the highest crystallinity was obtained after a 1 h reaction time at 95 °C.

Different loadings of Fe^{3+}were used in the precursor solution: 10, 15, 20, 25, and 30 wt % (herein referred to as FC-10, FC-15, FC-20, FC-25, and FC-30, respectively, where FC stands for Fe-grafted CAU-28) were used to synthesize the materials under the optimized reaction conditions (95 °C, 1 h). X-ray fluorescence (XRF) spectroscopy was performed to determine the Fe content of the solid MOF materials, which revealed that the amount of Fe^{3+} in solution during synthesis does not directly translate to the actual Fe loading in the MOFs. With increasing Fe^{3+} in the synthesis precursor solution, the Fe concentration in the MOF also increased; however, a loading of only 5.5% (by mass) was observed in case of FC-25 (i.e., from an intended 25 wt % Fe^{3+} in solution during synthesis, Figure 2a and Table S1). The remainder of the iron presumably remains in solution after the reaction and is removed by washing.

Increasing the precursor concentration of Fe^{3+} further to 30 wt % resulted in the breakdown of the MOF structure, as observed from the loss of crystallinity in the powder X-ray diffraction (PXRD) pattern of FC-30 (Figure S2). The PXRD patterns of the other FC materials (FC-10, FC-15, FC-20, and FC-25) are consistent with that of simulated bare CAU-28 confirming the preservation of the hexagonal crystal structure (Figure 2b and Figure S3); however, a shift of the major reflections ((002) and (200)) toward higher 2θ angles is observed with an increasing Fe content (Figure 2b). This attests to the inclusion of Fe species in the MOF, resulting in the alteration of the unit cell volume (Figure 2b). The crystallinity of FC-25 (which emerged as the best catalyst as discussed in later sections) is also comparatively lower than that of bare CAU-28, which indicates successful incorporation of Fe species in the MOF (Figure S4), as expected when dopants or substituents are added to a material.[34,35] Furthermore, profile fitting of the PXRD pattern of FC-25 (Figure S5 and Table S2) reveals a lower unit cell volume of 12990(7) $Å^3$, as compared to the volume of parent CAU-28 (13,398 $Å^3$), further attesting to the presence of Fe species in the MOF structure.

To gain further insight into the effect of Fe inclusion on CAU-28, the BET surface area analyses were conducted on the nitrogen adsorption isotherms of the materials (Figure 2c).

https://doi.org/10.1021/acssuschemeng.3c08564
ACS Sustainable Chem. Eng. 2024, 12, 5575−5585

The surface area shows a decrease with the inclusion of Fe into the MOF as compared to parent CAU-28 (Table S3).[36] The reduction of the surface area with an increasing Fe loading indicates that the Fe species may be present within the channels of the structure or blocking the entrance to pores, rather than inclusion in the MOF framework. The hexagonal rod-shaped crystallite morphology is retained as observed from the field-emission scanning electron microscopy (FESEM) image of FC-25 in Figure S6a, while the corresponding energy-dispersive X-ray (EDX) elemental maps showed a homogeneous distribution of C, Zr, and O. However, no Fe could be detected from the elemental maps, which is likely due to the very low concentration of Fe (beyond the detection limit of EDX) and, given the surface sensitivity of the technique, the likely absence of any Fe species on the MOF surface. The average diameter of an individual FC-25 nanorod was determined to be 342 ± 68 nm (Figure S6b). Solid-state UV−vis spectroscopy was also carried out to identify the possible formation of any iron oxide in the material (Figure S7). This revealed two dominant broad absorption bands at ∼280 and ∼350 nm (Figure S7a). The band at the lower wavelength corresponds to the π to π^* electron transfer due to the furan ring of the FDC ligand, whereas the second band is assigned to be due to the presence of the grafted iron, as was also seen in the UV−vis spectrum of Fe-grafted UiO-66 that contains the same Zr_6 building unit.[37,38] The solid-state UV−vis spectra of pristine Fe_2O_3 showed an absorption onset at ∼690 nm, while Fe_3O_4 did not show any strong absorption signal (Figure S7b). Therefore, no signature of iron oxides was found, confirming the absence of such species in the catalyst system.

Thermogravimetric analysis (TGA) was carried out to determine the thermal stability of the FC systems, which is essential for catalytic applications (Figure S8). The TGA profile for the different FC systems was similar and comparable to that of bare CAU-28, which has a chemical formula of $[Zr_6O_4(OH)_4(FDC)_4(OH)_4(H_2O)_4]$. Three different weight-loss stages were observed. The first step corresponds to the loss of occluded water, the second weight-loss step can be attributed to the dihydroxylation of Zr nodes ($[Zr_6O_4(OH)_4]$), and the third step can be assigned to the combustion of FDC organic linkers.[34,39] The observed and expected mass-loss values for parent CAU-28 and FC-25 are provided in Table S4. It is noteworthy that the residual mass after TGA analysis for FC-25 was slightly higher than that of bare CAU-28, consistent with the presence of Fe. In order to eliminate the possibility of Fe species being present on the surface of the MOF, X-ray photoelectron spectroscopy (XPS) was used. As expected, XPS showed the presence of Zr (Zr 3d peak in Figure S9), but no Fe was detected, which confirmed the absence of any Fe species at the surface of the FC catalysts.

While the above-mentioned analyses provide sufficient evidence of the incorporation of Fe species within the MOF, the exact coordination environment, oxidation state, and nature of bonding of the Fe species remain unclear. To resolve this, the Fe K-edge X-ray absorption near-edge structure (XANES) and extended X-ray absorption fine structure (EXAFS) were used to probe the local electronic and coordination environment of Fe (see Methods for details). As seen from the XANES spectra (Figure S10), the absorption edge position of the FC systems was similar in nature to octahedral Fe^{3+} in α-Fe_2O_3 (used as a reference), although the shape of the near edge differs, implying that the local environment is not identical. The experimental and fitted *k*-weighted EXAFS spectra and the corresponding magnitude of Fourier transform (FT) *R*-space are shown in Figure 2d,e (with results of the fitting in Table S5). The EXAFS spectra of FC-25 can be fitted by a single shell of oxygens at ∼2.06 Å, which is notably different from Fe_2O_3 where additional shells of atoms are clearly detected, with notable Fe−Fe distances of 2.57 Å. Therefore, it can be clearly concluded that the environment of the Fe inside the CAU-28 MOF does not resemble Fe_2O_3 (Figure S11) and that the Fe is coordinated to six oxygens with the absence of longer atomic correlations. These observations suggest that Fe is not doped into the Zr clusters of CAU-28 but is grafted onto the clusters inside the MOF as an octahedral Fe^{3+} complex without any long-range order (Figure 2f). Moreover, the fact that the Fe could not be easily removed from the MOFs post catalysis (discussed in the Supporting Information) further attests that it is chemically bound or grafted to the Zr cluster in the MOF channels. IR spectra for the bare MOF and FC-25 reveal no difference in the vibrational stretching, which supports the idea of iron being present as a grafted unit and not coordinated to the ligand (Figure S12). A similar situation has been observed with Fe incorporation in the MOF UiO-66 containing the same ($[Zr_6O_4(OH)_4]$) clusters, giving further weight to our hypothesis of Fe grafting in the FC materials.[38]

The different FC catalysts were utilized for the catalytic oxidation of HMF under base-free conditions. To explore and understand the conversion efficiencies, product distribution, and selectivity, two different catalytic approaches were used: conventional solvothermal heating and microwave-assisted conversion (discussed below), and the reaction products were analyzed and quantified using ^{1}H nuclear magnetic resonance (^{1}H NMR) spectroscopy. This method was chosen to allow for unambiguous identification of all products as well as accurate determination of conversion and selectivity.

The conventional catalytic HMF conversion reactions using conventional heating were initially explored using the different FC catalysts (with varying Fe contents) under a reaction temperature of 60 °C in an aqueous medium (without base) with concentrations of the *t*-butyl hydroperoxide (*t*-BuOOH) oxidant (8 eqv) and the (2,2,6,6-tetramethylpiperidin-1-yl)oxyl (TEMPO) cocatalyst (1.2 eqv) for 24 h (see Methods for details). Among the four systems, FC-25, having the highest Fe content (∼5% as determined using XRF spectroscopy, see above), emerged as the best catalyst showing the highest HMF conversion (∼90%) along with maximum FDCA and FFCA yields of 23 and 39%, respectively (Figure S13 and Table S6). The reaction conditions were optimized for FC-25 by varying the time, temperature, and concentrations of the reagents used, and it was found that 60 °C, 48 h, 8 eqv of *t*-BuOOH, and 1.2 eqv of TEMPO were optimum for the HMF conversion reaction with the highest FDCA yield of 38 ± 2%. Higher temperatures decreased the catalytic activity of FC-25 with reduced HMF conversion (87.4 and 87.3% at 70 and 80 °C, respectively) and lower FDCA yields (9.6 and 17.6% at 70 and 80 °C, respectively; Figure S14 and Table S7). The reactions performed at a lower temperature of 50 °C also did not lead to appreciable HMF conversion. The formation of unaccounted byproducts at elevated temperatures may be attributed to the thermally induced degradation of HMF and/or its intermediate oxidation products.[40] The influence of the cocatalyst TEMPO and the oxidant *t*-BuOOH on the catalytic process was also explored. Reactions carried out by varying the

https://doi.org/10.1021/acssuschemeng.3c08564
ACS Sustainable Chem. Eng. 2024, 12, 5575−5585

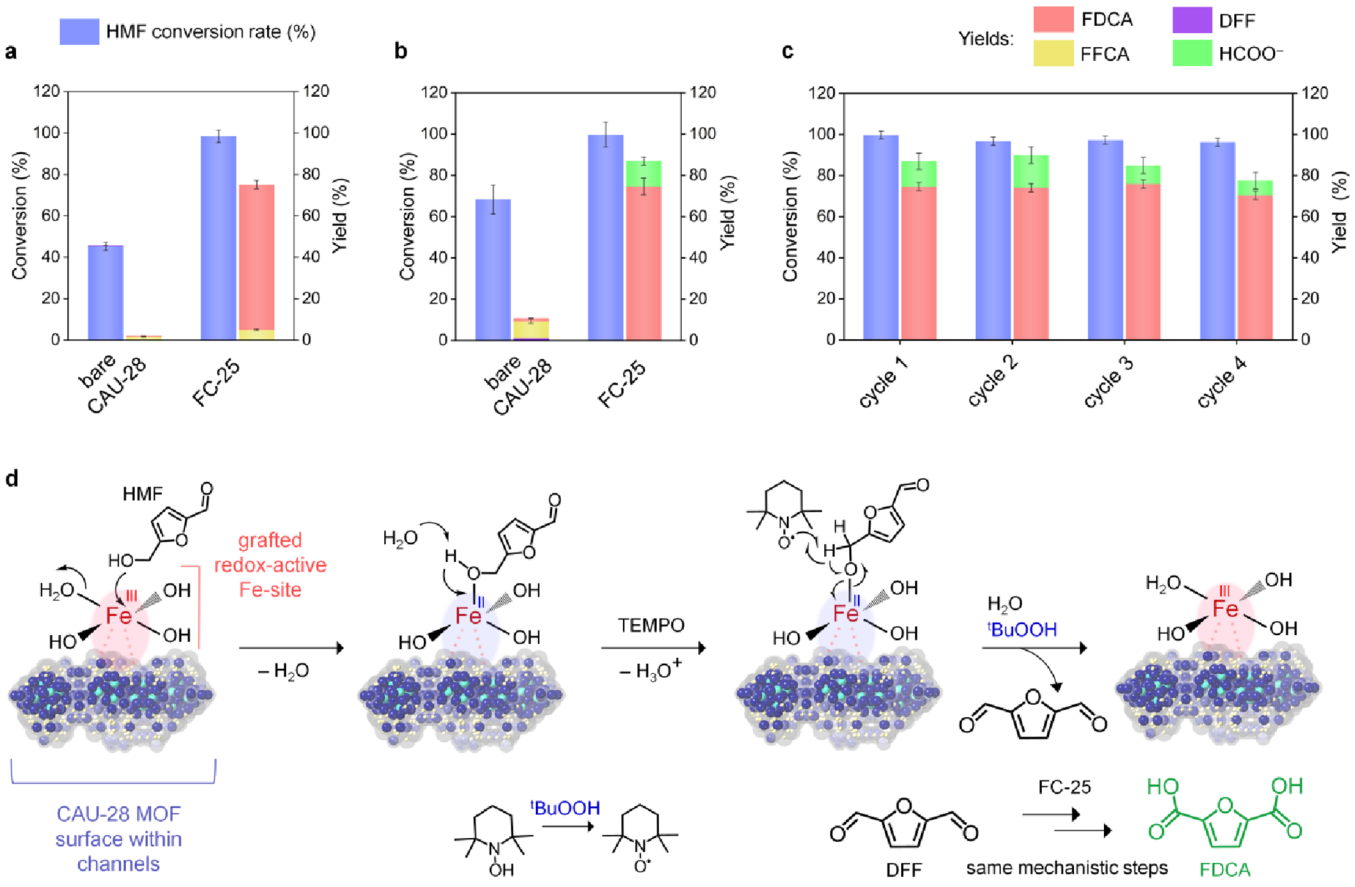

Figure 3. Catalytic conversion of HMF to FDCA using the FC-25 system. (a,b) Plot showing the HMF conversion rates and product yields with bare CAU-28 and FC-25 catalysts using optimized conventional heating (a) and microwave-assisted (b) methods under stepwise oxidant addition. (c) Recyclability tests of FC-25 toward selective HMF conditions using the microwave-assisted method. (d) Proposed reaction mechanism for HMF oxidation to FDCA over redox-active Fe species in the FC-25 system under base-free aqueous conditions. In each reaction, 30 mg of the FC catalyst, 3 mL of aqueous HMF solution, 1.32 mL of *t*-BuOOH (8 eqv), and 188 mg of TEMPO (1.2 eqv) were used at temperatures of 50−80 °C (conventional heating) or 100−140 °C (microwave heating); see the Methods section.

TEMPO amount (0.3, 0.6, and 1.2 eqv) at 60 °C (using 8 eqv of *t*-BuOOH) revealed that with an increasing TEMPO concentration, the HMF conversion also increased and already reached 90% with 1.2 eqv of TEMPO after 24 h (Figure S15 and Table S8). Similarly, catalytic tests were carried out by varying the concentration of the oxidant *t*-BuOOH (4, 8, and 16 eqv) while keeping other parameters constant (60 °C, 24 h, and 1.2 eqv of TEMPO; Figure S16 and Table S9). In this case, interestingly, it was observed that 8 eqv of *t*-BuOOH gave the optimum HMF conversion rate, while a further increase in the concentration of *t*-BuOOH to 16 eqv resulted in a drop in the catalytic activity. Additionally, control exclusion experiments performed by eliminating one reaction parameter at a time did not result in high conversion efficiencies and product yields (Figure S17). The possibility of FDCA being produced via the disassembly of the MOF catalyst was eliminated by conducting a control experiment under identical conditions but without the HMF substrate, which revealed no traces of FDCA in the postcatalytic solution as evidenced by solution ^{1}H NMR (Figure S18). The recyclability tests performed with FC-25 under optimized conditions revealed that the FDCA selectivity was well-maintained over four cycles, with only a slight drop in HMF conversion (Figure S19). This minor decrease could be due to the accumulation of insoluble byproducts blocking the active sites of the catalyst.[28] Postcatalytic PXRD and FESEM characterization of the FC-25 catalyst confirmed the retention of the material's structure and morphology as observed in Figure S20. Additionally, inductive coupled plasma-optical emission spectroscopy (ICP-OES) analysis of the reaction solution postcatalysis revealed negligible leaching of the metal species (~2.9% Fe and ~0.01% Zr) from the catalyst after 48 h, further indicating successful Fe grafting and durability of the catalyst under the conditions used.

To boost the FDCA production (and selectivity) under the conventional heating method, reactions were carried out under stepwise addition of the oxidant (total of the optimized fixed amount of 8 eqv using a syringe filter pump), and this was identified as the key factor for higher FDCA production using the FC-25 catalyst (Figure S21, see the Supporting Information for details). This approach increased the FDCA production by ~30%, yielding 70.01 ± 2% FDCA (and 4.95 ± 0.3% FFCA) after 48 h (Figure 3a). The role of redox-active grafted Fe species (within CAU-28 channels) to achieve efficient catalytic conversion of HMF to FDCA (and FFCA) was verified by comparing the catalytic activity of the pristine CAU-28 MOF under optimized conditions. As seen from Figure 3a, the parent CAU-28 (with no Fe grafting) showed negligible catalytic activity with poor HMF conversion and no significant production of either FDCA or FFCA. Moreover, reactions performed solely with solution Fe^{3+} species in the medium (using $FeCl_3$) instead of FC-25 also did not lead to

https://doi.org/10.1021/acssuschemeng.3c08564
ACS Sustainable Chem. Eng. 2024, 12, 5575−5585

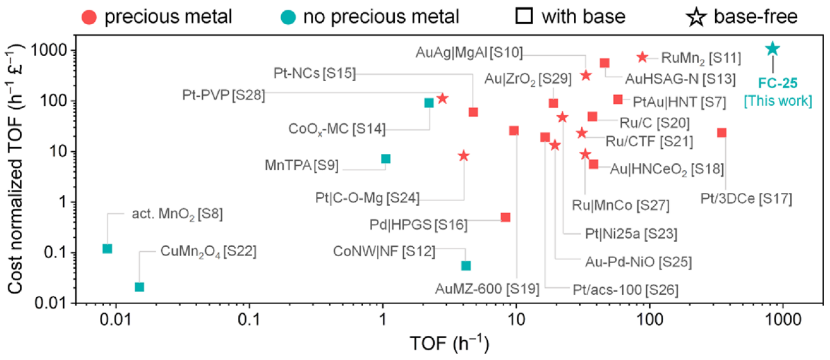

Figure 4. Performance and economic feasibility comparison of the FC-25 catalyst with existing state-of-the-art catalysts for HMF conversion. The plot depicts the TOFs and cost-normalized TOFs (based on catalyst reagent costs) of the different catalyst systems (all of which are either based on precious elements or the use of base in the reaction media), in comparison to the FC-25 catalyst achieving selective HMF to FDCA conversion under base-free aqueous conditions (optimized and best performing microwave-assisted approach). The FC-25 system shows the highest TOF and economic feasibility over existing approaches (see Table S12 for further details and the corresponding references).

satisfactory product formation (Figure S17). These results attest to the importance of grafted Fe^{3+} species for efficient HMF conversion via host−guest catalysis.

Although the conventional heating method facilitates the HMF oxidation reaction using FC catalysts, the selectivity of the desired product FDCA is still compromised with the intermediate FFCA not being fully converted during the process. Moreover, the conventional heating approach requires a long duration (48 h), which is not practical for the purpose of scalable FDCA production. Therefore, we explored microwave-assisted catalysis for HMF to FDCA conversion under the same optimized conditions to induce higher heating rates than conventional heating, thereby improving reaction kinetics, but which, to our knowledge, has not been used for HMF oxidation reactions.

The microwave-assisted reactions were carried out using the same optimized reagent concentrations (as used in conventional heating) at 120 °C for 1 h (the temperature and reaction duration were also optimized as seen from Figures S22 and S23 and Tables S10 and S11). Under these conditions, as evident from Figures S22 and S23, the HMF oxidation was highly selective toward FDCA production although full HMF conversion was not obtained. Therefore, similar to the conventional heating method, the microwave-assisted reactions were carried out with stepwise addition of *t*-BuOOH at regular time intervals of 10 min (rather than one-time addition at the beginning; see Methods) while keeping the final concentration (8 eqv) fixed over the entire reaction duration (1 h). This approach resulted in 100% HMF conversion within 1 h with a high FDCA yield of 74 ± 3% (Figure 3b). The remaining product identified was formic acid from the ring-opening rehydration of HMF, and no traces of FFCA were obtained, indicating complete conversion to the desired product.[41] The stepwise addition of the oxidant *t*-BuOOH ensured a sustained supply of the oxidant during catalysis, without it being degraded rapidly to water and *t*-butanol under microwave conditions. This was corroborated when the cocatalyst TEMPO was added in a stepwise manner with the initial one-time addition of *t*-BuOOH, which resulted in incomplete conversion of HMF (until the DFF stage) due to the rapid consumption/degradation of *t*-BuOOH at the initial stages of the catalytic reaction.

The FC-25 catalyst exhibited excellent recyclability over four catalytic cycles, maintaining a high HMF conversion rate and FDCA yield under microwave conditions (Figure 3c). The PXRD and FESEM analyses post recyclability tests attested to the structural integrity and durability of the FC-25 catalyst with no significant loss in crystallinity or morphological changes. The stability of the catalyst at higher temperatures in the microwave-heated reaction must be due to the rapid heating and short reaction time required, which is in contrast to the conventionally heated reaction, as discussed above. Furthermore, in order to assess the heterogeneity of the reaction and the durability of the catalyst, a hot filtration test was carried out after 30 min of the reaction. As from Figure S24, it is evident that without the catalyst, the reaction does not progress further, confirming the stability and activity of the grafted iron toward catalysis. The catalytic reaction was also carried out in the gram scale (1.5 g of the HMF substrate), and the FDCA obtained (1.04 g) was isolated and purified using recrystallization, thereby pointing toward the scalability of the overall process (Figure S25). The purity of the FDCA was further confirmed by measuring the TGA-DSC data and comparing it against the commercially available FDCA ligand (Figure S26).

Based on the experimental observations and considering a previous literature report on HMF conversion,[30] a plausible mechanism for the operation of the FC catalyst is proposed in Figure 3d. The redox-active, grafted Fe^{3+} site is crucial for HMF oxidation, where the loss of terminal water provides the Lewis acidity needed to bind substrate molecules as well as the redox activity to mediate the oxidation reactions. The presence of highly active grafted Fe^{3+} sites and the favorable substrate−catalyst interactions that the MOF provides plausibly eliminate the need for an additional base in the reaction media, which so far was not possible under conventional thermal catalytic conditions.

The various processes achieving HMF conversion that have already been reported (Table S12) mostly either rely on the use of precious-metal-based catalysts (such as Pt, Au, etc.) or the presence of base in the reaction media, making the overall approach unsustainable and expensive.[42−45] Many processes also suffer from additional limitations such as low production rates and poor catalytic turnovers.[46−48] The FC-25 catalyst, based on cheap and earth-abundant elements and a ligand from sustainable sources, emerges as a superior system achieving full HMF conversion and high FDCA selectivity under complete base-free aqueous conditions. The turnover

https://doi.org/10.1021/acssuschemeng.3c08564
ACS Sustainable Chem. Eng. 2024, 12, 5575−5585

frequency (TOF) calculated for the FC-25 system under microwave-assisted HMF conversion was 834.5 h^{-1}, which surpasses all reported catalyst systems for HMF conversion as shown in Figure 4.

To appreciate the economic viability of the catalytic process, the cost-normalized TOF (TOF normalized with respect to the catalyst cost) was calculated for FC-25 and compared to the existing state-of-the-art catalytic systems (Figure 4; see the Supporting Information for details). The cost-normalized TOF for FC-25 was also higher than all representative catalytic systems/processes based on precious metals or base additives, indicating the high performance and economic advantage of the green FC-25 catalyst toward scalable and sustainable FDCA production from HMF.

To demonstrate the circularity of our HMF conversion process and further establish the real-world applicability and potential commercial advantages of our process, the catalytically derived FDCA was used (without additional purification steps) to produce a fresh batch of CAU-28 MOFs and synthesize the robust, green PEF bioplastics. This was possible owing to the high selectivity of the microwave-assisted process toward FDCA production with significant yields (~70−80%) in the postcatalytic solution and the absence of any FFCA intermediates.

For the construction of CAU-28 MOFs, the reaction solution post microwave-assisted catalysis (under optimized conditions; discussed above) using FC-25 was centrifuged, and the supernatant was separated from the solid recyclable catalyst (discussed above). The supernatant, primarily containing FDCA, along with traces of the byproduct formic acid was directly used for the synthesis of CAU-28 MOFs following the addition of a Zr^{4+} salt under optimized synthetic conditions (see Methods for details). The obtained solid product was characterized using PXRD, which showed the characteristic reflections of CAU-28 (Figure S26a). Moreover, FESEM analyses of the product showed a similar hexagonal rod-shaped morphology to that observed in the case of the FC systems, confirming the successful synthesis of CAU-28.

For PEF synthesis, the catalytically derived FDCA was directly used for the polymerization reaction in the presence of the secondary monomer ethylene glycol and the polymerization agent titanium isopropoxide under nitrogen flow at 190 °C (see Methods for details). The successful formation of the biodegradable polymer was confirmed using PXRD, ^{1}H NMR spectroscopy, and differential scanning calorimetry (DSC) studies (Figure S26b). The PXRD pattern and ^{1}H NMR spectra revealed the characteristic signatures of the PEF bioplastic, similar to previous reports. The DSC data indicate the biopolymer to be semicrystalline with a glass transition temperature (T_g) of ~73.6 °C and a melting temperature (T_m) of ~192 °C, which is in accordance previous reports on PEF.[49−52] Size-exclusion chromatography gives a number-average molecular weight M_n > 38 kg/mol with a polydispersity index of 1.7 indicating moderate distribution and in agreement with Rosenboom et al. (Figure S27).[53]

CONCLUSIONS

We have reported not only a catalyst that functions exceptionally well without the use of excessive quantities of base, without expensive reagents, and without the application of pressure but one that is constructed from a ligand sourced from sustainable precursors and containing a combination of benign metals. The advantage of our approach is the simplicity of the one-pot reaction system compared to when oxygen gas is used as an oxidant, which typically must be continuously fed through the reagent mixture. We have demonstrated grafting of catalytically active Fe^{3+} sites on the Zr cluster of FDCA-based CAU-28 MOFs using a mild solvothermal method. The structural modification is supported by various analytical approaches, with Fe K-edge EXAFS analysis confirming isolated redox centers and PXRD showing retention of crystallinity with a contraction of the unit cell volume in response to the Fe inclusion. The work demonstrates the first approach of grafting redox-active species on MOFs constructed from sustainably sourced ligands and utilizing them as efficient catalysts for selective HMF conversion to the platform chemical FDCA under base-free aqueous conditions. The optimized catalysis shows remarkably high catalytic activity toward HMF conversion via conventional heating and microwave-assisted methods. Under optimized microwave reaction conditions, the best catalyst achieves 100% HMF conversion and a 70−80% FDCA yield in the gram scale within 1 h, with no residual intermediates such as DFF and FFCA. The TOF and cost-normalized TOF of our best catalyst reached 834.5 and 1069.87 h^{-1} £$^{-1}$, respectively, surpassing the state-of-the-art catalyst systems/processes for HMF conversion based on precious metals or unsustainable base additives in their reaction media. The catalytically derived FDCA was also used directly for the synthesis of pristine CAU-28 MOFs and the green bioplastic PEF, thereby introducing circularity and presenting a demonstration of economic feasibility of HMF valorization using our scalable, efficient, and sustainable catalytic process.

EXPERIMENTAL SECTION

Materials. 5-Hydroxymethylfural (HMF, 99%, Sigma-Aldrich), *tert*-butyl hydroperoxide (*t*-BuOOH, 70% aq., 98%, Sigma-Aldrich), furan-2,5-dicarboxylic acid (FDCA, 98%, Alfa Aesar), deuterium oxide (D_2O, 99.96%, Sigma-Aldrich), glacial acetic acid (Fischer Scientific), zirconyl chloride octahydrate ($ZrOCl_2{\cdot}8H_2O$, 98%, Alfa Aesar), isopropyl alcohol ($(CH_3)_2CHOH$, >99.7%, Sigma-Aldrich), deionized water, iron chloride hexahydrate ($FeCl_3{\cdot}6H_2O$, 99%, Merck), iron oxide (Fe_2O_3, Alfa Aesar), iron oxide (Fe_3O_4, 99.99%, Sigma-Aldrich), TEMPO (98%, Sigma-Aldrich), ethanol (99.8%, VWR), 1,4-dioxane (95%, Fischer Scientific), ethylene glycol, titanium isopropoxide (97%, Sigma-Aldrich), trifluoroacetic acid (99%, Scientific Laboratory Supplies Ltd.), and chloroform (99%, VWR) were utilized. All of the reagents were used as received without further purification.

Methods. *Synthesis of FC Systems.* The parent CAU-28 was prepared using a modified approach from that in the literature. $ZrOCl_2{\cdot}8H_2O$ (60 mg) and FDCA (45 mg) were placed together in a glass reaction vial and then dissolved in an acetic acid (0.7 mL) and water (0.8 mL) mixture by volume under continuous stirring at room temperature. Subsequently, the reaction mixture was transferred to a round-bottom flask and heated in an oil bath at 95 °C for 1 h. The resultant solution was then redispersed in ethanol twice and centrifuged at 4000 rpm. The obtained product was dried at 70 °C overnight in air. The FC systems were prepared by gradually increasing the Fe^{3+} concentration in the reaction medium for the usual CAU-28 synthesis. For the sample with the highest Fe grafting (FC-25), 15 mg of $FeCl_3{\cdot}6H_2O$ was added into the precursor solution along with $ZrOCl_2{\cdot}8H_2O$ (45 mg) and FDCA (45 mg) followed by heating in an oil bath at 95 °C for 1 h. The product was washed in ethanol, isolated using centrifugation at 4000 rpm, and dried overnight at 70 °C in air.

Catalytic HMF Conversion Using Conventional Oil-Bath Heating. A stock solution of HMF was prepared by dissolving 800 mg of HMF in 16 mL of deionized water to reach a final concentration of 6.31 M. Catalysis was carried out and studied in

https://doi.org/10.1021/acssuschemeng.3c08564
ACS Sustainable Chem. Eng. 2024, 12, 5575−5585

30 mL DURAN® tubes. In a typical experiment, 30 mg of the FC catalyst, 3 mL of aqueous HMF solution, 1.32 mL of *t*-BuOOH (8 eqv), and 188 mg of TEMPO (1.2 eqv) were added into the reaction vial. The solution was then heated in an oil bath at a chosen temperature (50, 60, 70, or 80 °C) for a particular duration (24, 48, or 72 h) under constant stirring. For preventing rapid oxidant consumption/degradation and achieving higher FDCA yields, 8 eqv of the oxidant *t*-BuOOH was added stepwise at regular time intervals using a syringe pump. After the completion of the reaction, the reaction vial was cooled to room temperature for further analysis and determination of product yield. ^{1}H NMR analysis of the solution diluted with D_2O was carried out by using 1,4-dioxane as an internal standard. The control experiments were carried out without the HMF substrate to observe any leaching of FDCA from the framework of the FC catalyst during the catalytic process. The conversion rate of HMF and the yields of DFF, FFCA, and FDCA were quantified using ^{1}H NMR spectroscopy and calculated using the following equations:

$$\text{conversion}(\%) = \frac{\text{initial moles of HMF} - \text{final moles of HMF}}{\text{initial moles of HMF}} \times 100 \quad (1)$$

$$\text{yield}(\%) = \frac{\text{moles of the products(DFF, FFCA, and FDCA)}}{\text{initial moles of HMF}} \times 100 \quad (2)$$

Selective Conversion of HMF to FDCA Using Microwave-Assisted Catalysis. In a typical microwave-assisted reaction, 150 mg of HMF, 30 mg of the FC catalyst, 1.32 mL of *t*-BuOOH, and 188 mg of TEMPO were loaded into a 30 mL reaction vial (G30). Three mL of water was added before it was placed in an Anton Paar 200 microwave reactor and exposed to microwave power (100 W) under vigorous stirring at 100−140 °C for a particular time, with 4 bar pressure generated. Similar to the conventional heating method, for minimizing rapid oxidant consumption/degradation and improving FDCA yields, *t*-BuOOH (total of 8 eqv optimized concentration) was added at periodic intervals of 10 min. The mixture was heated at 120 °C for 1 h under optimized conditions. The resultant mixture and products obtained were analyzed and quantified using ^{1}H NMR spectroscopy.

Recyclability Tests for the FC-25 Catalyst. The recyclability tests for the best performing FC-25 catalyst were carried out using both conventional heating and microwave-assisted catalysis for five consecutive cycles (first run + additional (1−4) cycles). In both scenarios, the FC-25 catalyst was collected using filtration, washed with water and isopropanol, and reused for the next catalytic cycle without any reactivation steps. After five cycles, the stability and durability of the catalyst were determined using postcatalytic characterization methods (PXRD and FESEM).

Hot Filtration Test. During this test, the catalyst was separated from the reaction by filtration while hot after 30 min of reaction progression, and the resulting solution was kept under the unaltered reaction condition; at every 10 min, the yield was monitored by ^{1}H NMR.

Purification of Catalytically Derived FDCA. The postcatalysis solution containing the FDCA product (from the optimized microwave-assisted method) was first centrifuged to separate the solid FC-25 catalyst. Thereafter, the resultant solution was poured into a vial, and the residual oxidant layer was carefully removed from the top. The solution was next heated (100.8 °C) with the addition of an appropriate amount of $NaHCO_3$, until all the liquid evaporated leaving behind the solid product. The solid product was collected, soaked in 1 M HCl for 30 min, and subsequently washed and dried. Finally, the FDCA product was isolated using recrystallization to remove any impurities, dried, and characterized.

Construction of the CAU-28 MOF Using Catalytically Derived FDCA. The CAU-28 MOF was synthesized in a single pot from the postcatalytic solution (from the best performing microwave-assisted method using the FC-25 catalyst). After separating the FC-25 catalyst from the postcatalytic solution using centrifugation at 4000 rpm for 10 min, the solution was kept unperturbed at room temperature for 30 min for the deep-yellow oxidant layer to separate out on the top of the aqueous layer. The oxidant layer was then carefully removed using a pipette. This was followed by the addition of $ZrOCl_2{\cdot}8H_2O$ and acetone to the solution, which was then heated to 95 °C for 1 h. The solid product (CAU-28 MOF) obtained was centrifuged, washed with water and ethanol, and characterized.

Synthesis of Bioplastic PEF from the Catalytically Derived FDCA. Following a similar approach to that above, the separated solution (postcatalysis and after TEMPO removal) was transferred to a three-neck round-bottom flask. Thereafter, an appropriate amount of ethylene glycol and titanium isopropoxide (polymerization agent) was added according to PEF synthesis protocols reported previously. The resultant solution was first heated at 190 °C for 4 h and then at 200 °C under an inert atmosphere. Finally, the solid semicrystalline product obtained was isolated for further analysis.

Materials Characterization. PXRD patterns were recorded using a Siemens D5000 diffractometer with Cu Kα (λ = 1.5418 Å) radiation with data recorded in Bragg−Brentano mode over scattering angles (2θ) of 3 to 50°. The scan rate was maintained at 2θ = 1°/min for all measurements. Rietveld refinement against the PXRD patterns was performed using GSAS-II software to determine the unit cell parameters.[54] The atom coordinates were fixed at the expected values from the reported crystal structure, and the quality of the refinement was ascertained by tracking the descending values of a weighted average residual (R_{wp}) and goodness-of-fit (GOF) values. The morphology of the catalyst was characterized by a Zeiss Supra 55-VP FESEM. TEM images were recorded using a JEOL 2000 FX/JEOL ARM2000FX. XRF data were measured using a Rigaku Primus IV wavelength-dispersive X-ray fluorescence spectrometer (WDXRF) equipped with a 4 kW X-ray tube. The TGA analysis was performed using a Mettler Toledo TGA/DSC1 instrument where samples were heated in air from 25 to 1000 °C with a heating rate of 10 °C/min. N_2 adsorption isotherms were measured at 77 K using a Micromeritics ASAP2020 apparatus, with the sample pretreated under vacuum at 120 °C for 3 h to remove water. The BET method was utilized to calculate the apparent surface area. ICP-OES measurements were performed using a Varian Vista MPX ICP-OES system by Medac Ltd. Solid-state UV−vis spectroscopy analysis was performed using a Shimadzu UV-2600 spectrophotometer. XPS was performed using a Kratos AXIS Ultra DLD. Sputtering was carried out via a Minibeam ion gun (Kratos Analytical) with a beam of 4 keV Ar^+ ions incident on the 3 × 3 cm^2 sample area. The XPS results were calibrated using the C 1s peak at 284.8 eV, which was employed to deconvolute the Fe 2p, Zr 3d, and O 1s peaks using the Shirley-type baseline and an iterative least-squares optimization algorithm. The XAS measurements were performed at the beamline B18 of the Diamond Light Source. Samples were pressed into pellets approximately 1 mm thick to optimize absorption measurements, diluted with cellulose powder in the case of the Fe_2O_3 reference.[55] Incident X-ray wavelengths were selected using a fixed-exit double-crystal Si (111) monochromator, and data were collected in the fluorescence mode (36 element Ge detector) before being normalized using software ATHENA to produce XANES and extended X-ray absorption fine structure (EXAFS) spectra. The k^3-weighted EXAFS spectra were modeled using ARTEMIS software, which uses the FEFF code for the calculation of phase shifts and effective scattering amplitudes, with starting structural models produced from published crystal structures to refine interatomic distances and thermal parameters.[56] ^{1}H NMR analysis was done with a Bruker Avance III HD 300 MHz instrument. Size-exclusion chromatography (SEC) characterization of the PEF was carried out using $CHCl_3$ as the eluent with an Agilent 1260 Infinity II MDS instrument equipped with differential refractive index (DRI), viscometry (VS), dual-angle light scatter (LS), and multiple-wavelength UV detectors. The system was equipped with 2× PLgel Mixed C columns (300 × 7.5 mm) and a PLgel 5 μm guard column. The eluent was run at 1 mL min^{-1} at 30 °C. Poly(methyl methacrylate) calibrants (Agilent EasiVials) were used to create a third-order calibration between 1,591,000 and 558 g mol^{-1}. Prior to injecting, the sample was prepared in a mixture of 2,2,2-trichloroethanol and phenol, heated at 150 °C for 1 h, and filtered

https://doi.org/10.1021/acssuschemeng.3c08564
ACS Sustainable Chem. Eng. 2024, 12, 5575−5585

through a 5 mm stainless-steel filter using a hot filtration device, PL-SP260 VS.

Quantitative ^{1}H NMR Spectroscopy. Samples were spiked with a known quantity of an internal standard (1,4-dioxane). The quantity of the analyte in the sample was calculated using eq 3 as shown below:

$$m_{\text{analyte}} = \frac{(M_{\text{analyte}} \times I_{\text{analyte}} \times N_{\text{standard}})}{(M_{\text{standard}} \times I_{\text{standard}} \times N_{\text{analyte}})} \times m_{\text{standard}} \quad (3)$$

where I_{analyte} is the integral of the analyte peak, N_{analyte} is the number of protons corresponding to the analyte peak, M_{analyte} is the molar mass of the analyte, and m_{standard} is the known mass of the standard in the sample.

■ ASSOCIATED CONTENT

Data Availability Statement

The data that support the findings detailed in this study are available in the article and its Supporting Information or from the corresponding author upon reasonable request.

Supporting Information

The Supporting Information is available free of charge at https://pubs.acs.org/doi/10.1021/acssuschemeng.3c08564.

PXRD patterns, UV−vis spectroscopy, XPS, TGA, Fe K-edge XANES, HMF oxidation parameter variation, ^{1}H NMR, recyclability measurement, postrecyclability analysis, microwave measurement variation, hot filtration test, TGA-DSC, PEF characterization, and comparison of FC-25 with state-of-the-art representative catalysts (PDF)

■ AUTHOR INFORMATION

Corresponding Author

Richard I. Walton − *Department of Chemistry, University of Warwick, Coventry CV4 7AL, U.K.;* orcid.org/0000-0001-9706-2774; Email: r.i.walton@warwick.ac.uk

Authors

Satarupa Das − *Department of Chemistry, University of Warwick, Coventry CV4 7AL, U.K.*

Giannantonio Cibin − *Diamond Light Source, Didcot OX11 ODE, U.K.*

Complete contact information is available at: https://pubs.acs.org/10.1021/acssuschemeng.3c08564

Author Contributions

R.I.W. supervised the project and conceived the idea. S.D. designed the experiments, synthesized the materials, performed all data analysis, and wrote the manuscript. G.C. measured the XAFS spectra. All the authors discussed the results, commented on the manuscript, and approved the final version of the manuscript.

Notes

The authors declare no competing financial interest.

■ ACKNOWLEDGMENTS

S.D. thanks the University of Warwick for the award of a Chancellor's International Scholarship. Some of the equipment used in this research was provided by the University of Warwick Research Technology Platforms, and we are grateful to Dr. Marc Walker, Katie Pickering, Dr. Thomas W. Chamberlain, Jasmine Clayton, Joe Gregory, Baiwen Zhao, Dr. Dan Lester, and Dr. Arkadios Marathianos for assistance with some of the measurements. We thank the Diamond Light Source for provision of beamtime for XAS via the Energy Materials Block Allocation Group SP14239.

■ REFERENCES

(1) Welsby, D.; Price, J.; Pye, S.; Ekins, P. Unextractable Fossil Fuels in a 1.5 °C World. *Nature* **2021**, *597* (7875), 230−234.

(2) Isikgor, F. H.; Becer, C. R. Lignocellulosic Biomass: A Sustainable Platform for the Production of Bio-Based Chemicals and Polymers. *Polymer Chem.* **2015**, *6* (25), 4497−4559.

(3) Bhattacharjee, S.; Rahaman, M.; Andrei, V.; Miller, M.; Rodríguez-Jiménez, S.; Lam, E.; Pornrungroj, C.; Reisner, E. Photoelectrochemical CO_2-To-Fuel Conversion with Simultaneous Plastic Reforming. *Nat. Synth.* **2023**, *2* (2), 182−192.

(4) Kar, S.; Zhou, Q.-Q.; Ben-David, Y.; Milstein, D. Catalytic Furfural/5-Hydroxymethyl Furfural Oxidation to Furoic Acid/Furan-2,5-Dicarboxylic Acid with H_2 Production Using Alkaline Water as the Formal Oxidant. *J. Am. Chem. Soc.* **2022**, *144* (3), 1288−1295.

(5) Fulignati, S.; Licursi, D.; Di Fidio, N.; Antonetti, C.; Galletti, A. M. R. Novel Challenges on the Catalytic Synthesis of 5-Hydroxymethylfurfural (HMF) from Real Feedstocks. *Catalysts* **2022**, *12* (12), 1664.

(6) Rosenfeld, C.; Konnerth, J.; Sailer-Kronlachner, W.; Solt, P.; Rosenau, T.; van Herwijnen, H. W. G. Current Situation of the Challenging Scale-up Development of Hydroxymethylfurfural Production. *ChemSusChem* **2020**, *13* (14), 3544−3564.

(7) Sajid, M.; Zhao, X.; Liu, D. Production of 2,5-Furandicarboxylic Acid (FDCA) from 5-Hydroxymethylfurfural (HMF): Recent Progress Focusing on the Chemical-Catalytic Routes. *Green Chem.* **2018**, *20* (24), 5427−5453.

(8) Tomás, R. A. F.; Bordado, J. C. M.; Gomes, J. F. P. *p*-Xylene Oxidation to Terephthalic Acid: A Literature Review Oriented toward Process Optimization and Development. *Chem. Rev.* **2013**, *113* (10), 7421−7469.

(9) Fei, X.; Wang, J.; Zhu, J.; Wang, X.; Liu, X. Biobased Poly(Ethylene 2,5-Furancoate): No Longer an Alternative, but an Irreplaceable Polyester in the Polymer Industry. *ACS Sustainable Chem. Eng.* **2020**, *8* (23), 8471−8485.

(10) Burgess, S. K.; Kriegel, R. M.; Koros, W. J. Carbon Dioxide Sorption and Transport in Amorphous Poly(Ethylene Furanoate). *Macromolecules* **2015**, *48* (7), 2184−2193.

(11) Kucherov, F. A.; Romashov, L. V.; Galkin, K. I.; Ananikov, V. P. Chemical Transformations of Biomass-Derived C6-Furanic Platform Chemicals for Sustainable Energy Research, Materials Science, and Synthetic Building Blocks. *ACS Sustainable Chem. Eng.* **2018**, *6* (7), 8064−8092.

(12) Totaro, G.; Sisti, L.; Marchese, P.; Colonna, M.; Romano, A.; Gioia, C.; Vannini, M.; Celli, A. Current Advances in the Sustainable Conversion of 5-Hydroxymethylfurfural into 2,5-Furandicarboxylic Acid. *ChemSusChem* **2022**, *15* (13), No. e202200501.

(13) Saha, B.; Dutta, S.; Abu-Omar, M. M. Aerobic Oxidation of 5-Hydroxylmethylfurfural with Homogeneous and Nanoparticulate Catalysts. *Catal. Sci. Technol.* **2012**, *2* (1), 79−81.

(14) Troiano, D.; Orsat, V.; Dumont, M. J. Status of Biocatalysis in the Production of 2,5-Furandicarboxylic Acid. *ACS Catal.* **2020**, *10* (16), 9145−9169.

(15) Ait Rass, H.; Essayem, N.; Besson, M. Selective Aqueous Phase Oxidation of 5-Hydroxymethylfurfural to 2,5-Furandicarboxylic Acid over Pt/c Catalysts: Influence of the Base and Effect of Bismuth Promotion. *Green Chem.* **2013**, *15* (8), 2240.

(16) Cheng, A.-B.; Shi, S.-S.; Li, Y.; Zong, M.-H.; Li, N. Biocatalytic Oxidation of Biobased Furan Aldehydes: Comparison of Toxicity and Inhibition of Furans toward a Whole-Cell Biocatalyst. *ACS Sustain. Chem. Eng.* **2020**, *8* (3), 1437−1444.

(17) Zhang, Z.; Deng, K. Recent Advances in the Catalytic Synthesis of 2,5-Furandicarboxylic Acid and Its Derivatives. *ACS Catal.* **2015**, *5* (11), 6529−6544.

(18) Zhao, D.; Rodriguez-Padron, D.; Triantafyllidis, K. S.; Wang, Y.; Luque, R.; Len, C. Microwave-Assisted Oxidation of Hydrox-

ymethyl Furfural to Added-Value Compounds over a Ruthenium-Based Catalyst. *ACS Sustainable Chem. Eng.* **2020**, *8* (8), 3091−3102.
(19) Rathod, P. V.; Jadhav, V. H. Efficient Method for Synthesis of 2,5-Furandicarboxylic Acid from 5-Hydroxymethylfurfural and Fructose Using Pd/CC Catalyst under Aqueous Conditions. *ACS Sustainable Chem. Eng.* **2018**, *6* (5), 5766−5771.
(20) Lei, D.; Yu, K.; Li, M.-R.; Wang, Y.; Wang, Q.; Liu, T.; Liu, P.; Lou, L.-L.; Wang, G.; Liu, S. Facet Effect of Single-Crystalline Pd Nanocrystals for Aerobic Oxidation of 5-Hydroxymethyl-2-Furfural. *ACS Catal.* **2017**, *7* (1), 421−432.
(21) Zhang, Z.; Zhen, J.; Liu, B.; Lv, K.; Deng, K. Selective Aerobic Oxidation of the Biomass-Derived Precursor 5-Hydroxymethylfurfural to 2,5-Furandicarboxylic Acid under Mild Conditions over a Magnetic Palladium Nanocatalyst. *Green Chem.* **2015**, *17* (2), 1308−1317.
(22) Woo, J.; Moon, B. C.; Lee, U.; Oh, H.-S.; Chae, K. H.; Jun, Y.; Min, B. K.; Lee, D. K. Collaborative Electrochemical Oxidation of the Alcohol and Aldehyde Groups of 5-Hydroxymethylfurfural by NiOOH and $Cu(OH)_2$ for Superior 2,5-Furandicarboxylic Acid Production. *ACS Catal.* **2022**, *12* (7), 4078−4091.
(23) Liu, H.; Jia, W.; Yu, X.; Tang, X.; Zeng, X.; Sun, Y.; Lei, T.; Fang, H.; Li, T.; Lin, L. Vitamin C-Assisted Synthesized Mn−Co Oxides with Improved Oxygen Vacancy Concentration: Boosting Lattice Oxygen Activity for the Air-Oxidation of 5-(Hydroxymethyl)-Furfural. *ACS Catal.* **2021**, *11* (13), 7828−7844.
(24) Al Ghatta, A.; Hallett, J. P. High Yield and Isolation of 2,5-Furandicarboxylic Acid from HMF and Sugars in Ionic Liquids, a New Prospective for the Establishment of a Scalable and Efficient Catalytic Route. *Green Chem.* **2022**, *24* (8), 3309−3313.
(25) Zhong, X.; Yuan, P.; Wei, Y.; Liu, D.; Losic, D.; Li, M. Coupling Natural Halloysite Nanotubes and Bimetallic Pt−Au Alloy Nanoparticles for Highly Efficient and Selective Oxidation of 5-Hydroxymethylfurfural to 2,5-Furandicarboxylic Acid. *ACS Appl. Mater. Interfaces* **2022**, *14* (3), 3949−3960.
(26) Donoeva, B.; Masoud, N.; de Jongh, P. E. Carbon Support Surface Effects in the Gold-Catalyzed Oxidation of 5-Hydroxymethylfurfural. *ACS Catal.* **2017**, *7* (7), 4581−4591.
(27) Furukawa, H.; Cordova, K. E.; O'Keeffe, M.; Yaghi, O. M. The Chemistry and Applications of Metal-Organic Frameworks. *Science* **2013**, *341* (6149), 1230444.
(28) Wang, C.; Liu, D.; Lin, W. Metal−Organic Frameworks as a Tunable Platform for Designing Functional Molecular Materials. *J. Am. Chem. Soc.* **2013**, *135* (36), 13222−13234.
(29) Yang, D.; Gates, B. C. Catalysis by Metal Organic Frameworks: Perspective and Suggestions for Future Research. *ACS Catal.* **2019**, *9* (3), 1779−1798.
(30) Chamberlain, T. W.; Degirmenci, V.; Walton, R. I. Oxidation of 5-Hydroxymethyl Furfural to 2,5-Furan Dicarboxylic Acid under Mild Aqueous Conditions Catalysed by MIL-100(Fe) Metal-Organic Framework. *ChemCatChem* **2022**, *14* (7), No. e202200135.
(31) Bao, L.; Sun, F.; Zhang, G.; Hu, T. Aerobic Oxidation of 5-Hydroxymethylfurfural to 2,5-Furandicarboxylic Acid over Holey 2D Mn_2O_3 Nanoflakes from a Mn-Based MOF. *ChemSusChem* **2020**, *13* (3), 548−555.
(32) Das, S.; Zhang, J.; Chamberlain, T. W.; Clarkson, G. J.; Walton, R. I. Nonredox CO_2 Fixation in Solvent-Free Conditions Using a Lewis Acid Metal−Organic Framework Constructed from a Sustainably Sourced Ligand. *Inorg. Chem.* **2022**, *61* (46), 18536−18544.
(33) Dreischarf, A. C.; Lammert, M.; Stock, N.; Reinsch, H. Green Synthesis of Zr-CAU-28: Structure and Properties of the First Zr-MOF Based on 2,5-Furandicarboxylic Acid. *Inorg. Chem.* **2017**, *56* (4), 2270−2277.
(34) Stawowy, M.; Ciesielski, R.; Maniecki, T.; Matus, K.; Łużny, R.; Trawczynski, J.; Silvestre-Albero, J.; Łamacz, A. CO_2 Hydrogenation to Methanol over Ce and Zr Containing UiO-66 and Cu/UiO-66. *Catalysts* **2020**, *10* (1), 39.
(35) Das, S.; Bhattacharjee, S.; Mondal, S.; Dutta, S.; Bothra, N.; Pati, S. K.; Bhattacharyya, S. Bimetallic Zero-Valent Alloy with Measured High-Valent Surface States to Reinforce the Bifunctional Activity in Rechargeable Zinc-Air Batteries. *ACS Sustainable Chem. Eng.* **2021**, *9* (44), 14868−14880.
(36) Du, T.; Wang, J.; Zhang, L.; Wang, S.; Yang, C.; Xie, L.; Liu, Z.; Ni, Y.; Xie, X.; Sun, J.; Zhang, W.; Wang, J. Missing-Linker Engineering of Eu (III)-Doped UiO-MOF for Enhanced Detection of Heavy Metal Ions. *Chem. Eng. J.* **2022**, *431*, No. 134050.
(37) Navin, C. V.; Krishna, K. S.; Theegala, C. S.; Kumar, C. S. S. R. Space and Time-Resolved Probing of Heterogeneous Catalysis Reactions Using Lab-On-a-Chip. *Nanoscale* **2016**, *8* (10), 5546−5551.
(38) Xu, C.; Pan, Y.; Wan, G.; Liu, H.; Wang, L.; Zhou, H.; Yu, S.-H.; Jiang, H.-L. Turning on Visible-Light Photocatalytic C−H Oxidation over Metal−Organic Frameworks by Introducing Metal-To-Cluster Charge Transfer. *J. Am. Chem. Soc.* **2019**, *141* (48), 19110−19117.
(39) Athar, M.; Rzepka, P.; Thoeny, D.; Ranocchiari, M.; van Bokhoven, J. A. Thermal Degradation of Defective High-Surface-Area UiO-66 in Different Gaseous Environments. *RSC Adv.* **2021**, *11* (61), 38849−38855.
(40) Nikolov, P.; Yaylayan, V. A. Thermal Decomposition of 5-(Hydroxymethyl)-2-Furaldehyde (HMF) and Its Further Transformations in the Presence of Glycine. *J. Agric. Food Chem.* **2011**, *59* (18), 10104−10113.
(41) Antonetti, C.; Licursi, D.; Fulignati, S.; Valentini, G.; Raspolli Galletti, A. New Frontiers in the Catalytic Synthesis of Levulinic Acid: From Sugars to Raw and Waste Biomass as Starting Feedstock. *Catalysts* **2016**, *6* (12), 196.
(42) Mishra, D. K.; Lee, H. J.; Kim, J.; Lee, H.-S.; Cho, J. K.; Suh, Y.-W.; Yi, Y.; Kim, Y. J. $MnCo_2O_4$ Spinel Supported Ruthenium Catalyst for Air-Oxidation of HMF to FDCA under Aqueous Phase and Base-Free Conditions. *Green Chem.* **2017**, *19* (7), 1619−1623.
(43) Liu, Y.; Ma, H.-Y.; Lei, D.; Lou, L.-L.; Liu, S.; Zhou, W.; Wang, G.-C.; Yu, K. Active Oxygen Species Promoted Catalytic Oxidation of 5-Hydroxymethyl-2-Furfural on Facet-Specific Pt Nanocrystals. *ACS Catal.* **2019**, *9* (9), 8306−8315.
(44) Liu, Z.; Tan, Y.; Li, J.; Li, X.; Xiao, Y.; Su, J.; Chen, X.; Qiao, B.; Ding, Y. Ag Substituted Au Clusters Supported on Mg-Al-Hydrotalcite for Highly Efficient Base-Free Aerobic Oxidation of 5-Hydroxymethylfurfural to 2,5-Furandicarboxylic Acid. *Green Chem.* **2022**, *24* (22), 8840−8852.
(45) Yang, W.; Yu, H.; Wang, B.; Wang, X.; Zhang, H.; Lei, D.; Lou, L.-L.; Yu, K.; Liu, S. Leveraging $Pt/Ce_{1-x}La_xO_{2-\delta}$ to Elucidate Interfacial Oxygen Vacancy Active Sites for Aerobic Oxidation of 5-Hydroxymethylfurfural. *ACS Appl. Mater. Interfaces* **2022**, *14* (33), 37667−37680.
(46) Hayashi, E.; Yamaguchi, Y.; Kamata, K.; Tsunoda, N.; Kumagai, Y.; Oba, F.; Hara, M. Effect of MnO_2 Crystal Structure on Aerobic Oxidation of 5-Hydroxymethylfurfural to 2,5-Furandicarboxylic Acid. *J. Am. Chem. Soc.* **2019**, *141* (2), 890−900.
(47) Liu, X.; Zhang, M.; Li, Z. CoO_x-MC (MC = Mesoporous Carbon) for Highly Efficient Oxidation of 5-Hydroxymethylfurfural (5-HMF) to 2,5-Furandicarboxylic Acid (FDCA). *ACS Sustainable Chem. Eng.* **2020**, *8* (12), 4801−4808.
(48) Wan, X.; Tang, N.; Xie, Q.; Zhao, S.; Zhou, C.; Dai, Y.; Yang, Y. A $CuMn_2O_4$ Spinel Oxide as a Superior Catalyst for the Aerobic Oxidation of 5-Hydroxymethylfurfural toward 2,5-Furandicarboxylic Acid in Aqueous Solvent. *Catal. Sci. Technol.* **2021**, *11* (4), 1497−1509.
(49) Maaskant, E.; van Es, D. S. Unexpected Susceptibility of Poly(Ethylene Furanoate) to UV Irradiation: A Warning Light for Furandicarboxylic Acid? *ACS Macro Lett.* **2021**, *10* (12), 1616−1621.
(50) Tsanaktsis, V.; Papageorgiou, D. G.; Exarhopoulos, S.; Bikiaris, D. N.; Papageorgiou, G. Z. Crystallization and Polymorphism of Poly(Ethylene Furanoate). *Cryst. Growth Des.* **2015**, *15* (11), 5505−5512.
(51) Maini, L.; Gigli, M.; Gazzano, M.; Lotti, N.; Bikiaris, D.; Papageorgiou, G. Structural Investigation of Poly(Ethylene Furanoate) Polymorphs. *Polymers* **2018**, *10* (3), 296.
(52) Papageorgiou, G. Z.; Tsanaktsis, V.; Bikiaris, D. N. Synthesis of Poly(Ethylene Furandicarboxylate) Polyester Using Monomers

https://doi.org/10.1021/acssuschemeng.3c08564
ACS Sustainable Chem. Eng. 2024, 12, 5575−5585

Derived from Renewable Resources: Thermal Behavior Comparison with PET and PEN. *Phys. Chem. Chem. Phys.* **2014**, *16* (17), 7946−7958.
(53) Rosenboom, J.-G.; Hohl, D. K.; Fleckenstein, P.; Storti, G.; Morbidelli, M. Bottle-Grade Polyethylene Furanoate from Ring-Opening Polymerisation of Cyclic Oligomers. *Nat. Commun.* **2018**, *9* (1), 2701.
(54) Toby, B. H.; Von Dreele, R. B. GSAS-II: The Genesis of a Modern Open-Source All Purpose Crystallography Software Package. *J. Appl. Crystallogr.* **2013**, *46* (2), 544−549.
(55) Dent, A. J.; Cibin, G.; Ramos, S.; Smith, A. D.; Scott, S. M.; Varandas, L.; Pearson, M. R.; Krumpa, N. A.; Jones, C. P.; Robbins, P. E. B18: A Core XAS Spectroscopy Beamline for Diamond. *J. Phys. Conf. Ser. Series* **2009**, *190*, No. 012039.
(56) Ravel, B.; Newville, M. Athena, Artemis, Hephaestus: Data Analysis for X-ray Absorption Spectroscopy Using IFEFFIT. *J. Synchrotron Radiat.* **2005**, *12* (4), 537−541.

https://doi.org/10.1021/acssuschemeng.3c08564
ACS Sustainable Chem. Eng. 2024, 12, 5575−5585